

Transport coefficients from the Nambu-Jona-Lasinio model for $SU(3)_f$

R. Marty,^{1,2,*} E. Bratkovskaya,^{1,2} W. Cassing,³ J. Aichelin,⁴ and H. Berrehrh¹

¹Frankfurt Institut for Advanced Studies, Johann Wolfgang Goethe Universität, Ruth-Moufang-Str. 1, 60438 Frankfurt am Main, Germany

²Institut for Theoretical Physics, Johann Wolfgang Goethe Universität, Max-von-Laue-Str. 1, 60438 Frankfurt am Main, Germany

³Institut für Theoretische Physik, Universität Gießen, Heinrich-Buff-Ring 16, 35392 Gießen, Germany

⁴Subatech, UMR 6457, IN2P3/CNRS, Université de Nantes, École des Mines de Nantes, 4 rue Alfred Kastler, 44307 Nantes cedex 3, France

We calculate the shear $\eta(T)$ and bulk viscosities $\zeta(T)$ as well as the electric conductivity $\sigma_e(T)$ and heat conductivity $\kappa(T)$ within the Nambu-Jona-Lasinio model for 3 flavors as a function of temperature as well as the entropy density $s(T)$, pressure $P(T)$ and speed of sound $c_s^2(T)$. We compare the results with other models such as the Polyakov-Nambu-Jona-Lasinio (PNJL) model and the dynamical quasiparticle model (DQPM) and confront these results with lattice QCD data whenever available. We find the NJL model to have a limited predictive power for the thermodynamic variables and various transport coefficients above the critical temperature whereas the PNJL model and DQPM show acceptable results for the quantities of interest.

PACS numbers: 11.10.Wx, 51.30.+i, 51.20.+d, 25.75.Nq

I. INTRODUCTION

For small momentum transfers quantum chromo-dynamics (QCD), the fundamental theory of strong interactions, can presently only be solved on a finite Euclidean lattice in thermodynamic equilibrium. Even this solution requires computer power in teraflops and many of the most interesting questions like the mass of hadrons at finite temperature and chemical potential as well as the properties of the constituents of deconfined matter and their interactions cannot be addressed presently accurately, either due to limited computer power or due to conceptual problems in particular at finite quark chemical potential μ .

Therefore one is strongly motivated to look for simpler models that incorporate essential features of QCD but are mathematically tractable. A candidate for this is the Nambu-Jona-Lasinio (NJL) model which is constructed in a way that its Lagrangian shares the symmetries of QCD –which are also observed in nature– but also the breaking of these symmetries. One of the most important of these symmetries is the chiral symmetry which is essential for the understanding of the hadron properties and their excitation spectra. We recall that the breaking of this symmetry is responsible for the dynamical creation of the fermion masses.

Whereas in former times the NJL approach has been mainly used to describe and to understand hadron properties at finite density and temperature, in recent times the interest has been extended to a systematic investigation of the properties and the interactions of quarks in deconfined matter especially at temperatures above the critical temperature T_c for the phase transition to deconfined matter. Without introducing additional parameters elastic scattering and hadronization cross sections for quarks and antiquarks have been calculated [1] which have more recently been used to model the expansion of a quark-antiquark plasma with initial conditions obtained

for nucleus-nucleus collisions at the Relativistic-Heavy-Ion Collider (RHIC) [2]. In order to compare this approach with other transport models, which study the expansion of the plasma created in ultra-relativistic heavy-ion collisions, it is useful to calculate and compare thermodynamic properties as well as transport coefficients in equilibrium as a function of the temperature T .

It is the purpose of this article to evaluate these quantities in the NJL model and to compare them with similar approaches such as the Polyakov-Nambu-Jona-Lasinio (PNJL) [3] and the dynamical-quasiparticle model (DQPM) [4–6]. The latter one is presently used in an independent transport approach which describes the time evolution of heavy-ion collisions from the creation of the partonic plasma until the registration of the final hadrons in the detectors, i.e. the Parton-Hadron-String-Dynamics (PHSD) approach [7–9]. Both models are quite different as far as the temperature dependence of the parton masses and the hadronization dynamics is concerned. It is therefore of interest to study whether these different ingredients lead to a different dynamics of the system. We will compare, as much as possible, all results also with available lattice QCD data.

II. THE NAMBU-JONA-LASINIO MODEL

Before the quantum chromo-dynamics (QCD) was formulated in 1973, Y. Nambu and G. Jona-Lasinio have advanced a model for strongly interacting fermions [10] –nucleons in their case– by a four point interaction. The use of the NJL model was extended to quarks and antiquarks only at the beginning of the ninety’s assuming the gluon degrees of freedom to be integrated out. The NJL Lagrangian presently used for our purpose for $SU(3)_f$ is taken from Ref. [11]:

$$\begin{aligned} \mathcal{L}_{NJL} = & \bar{\psi}(i\partial - m_0)\psi \\ & + G \sum_{a=0}^8 \left[(\bar{\psi}\lambda^a\psi)^2 + (\bar{\psi}i\gamma_5\lambda^a\psi)^2 \right] \\ & - K [\det\bar{\psi}(1 - \gamma_5)\psi + \det\bar{\psi}(1 + \gamma_5)\psi], \end{aligned} \quad (1)$$

* Email : marty@fias.uni-frankfurt.de

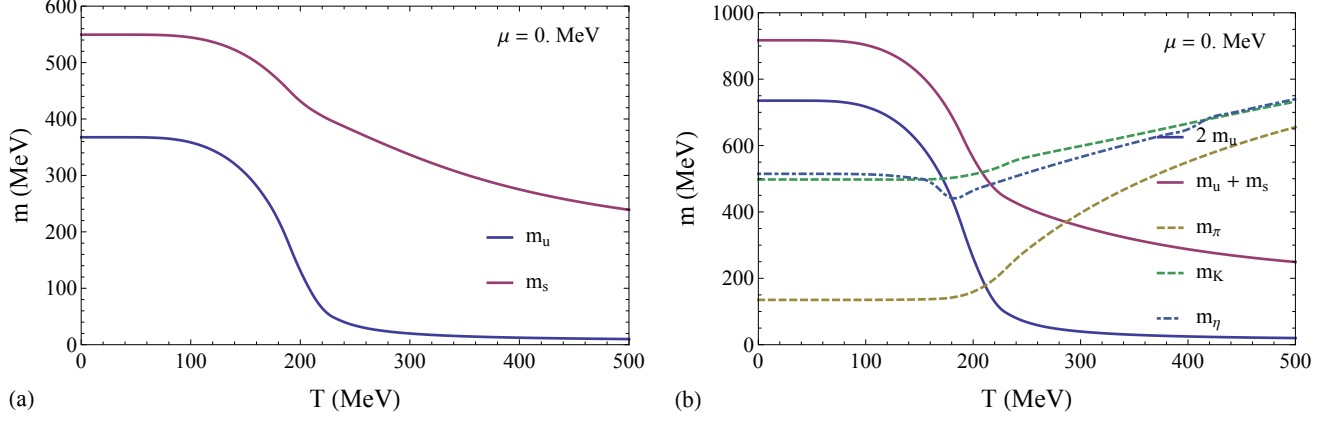


FIG. 1. Masses of quarks (a) and pseudoscalar mesons (b) as a function of the temperature T in the NJL model.

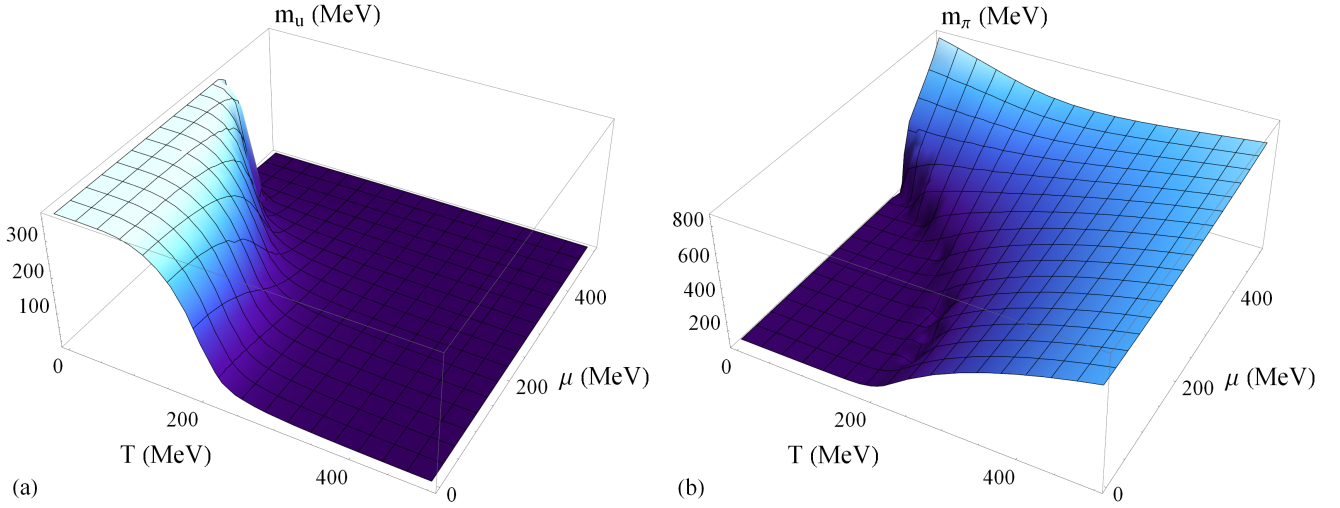


FIG. 2. Masses of u quarks (a) and π mesons (b) as a function of the temperature T and the quark chemical potential μ in the NJL model.

where $\psi = u, d, s$ is the quark field with three flavors ($N_f = 3$) and three colors ($N_c = 3$), λ^a are the flavor $SU(3)_f$ Gell-Mann matrices ($a = 0, 1, \dots, 8$), and G and K are coupling constants. The first line is the Lagrangian of freely moving quarks with a constituent mass m_0 . The second(third) line of Eq. (1) describes the 4(6) quark interaction. The symmetry group of the NJL model is the same as of QCD:

$$U(3)_L \otimes U(3)_R = SU_V(3) \otimes SU_A(3) \otimes U_V(1) \otimes U_A(1). \quad (2)$$

The chiral symmetry is spontaneously broken in vacuum and explicitly broken by the bare mass m_0 of quarks in Eq. (1). The well-known axial anomaly $U_A(1)$ is broken by the last term of Eq. (1) which relates to the 't Hooft mixing.

From this Lagrangian we can get effective masses for quarks. In the mean-field approximation they are given by

$$m_i = m_{0i} - 4G\langle\langle\bar{\psi}_i\psi_i\rangle\rangle + 2K\langle\langle\bar{\psi}_j\psi_j\rangle\rangle\langle\langle\bar{\psi}_k\psi_k\rangle\rangle, \quad (3)$$

with $i \neq j \neq k$ denoting the 3 possible flavors of quarks, and

$\langle\langle\bar{\psi}\psi\rangle\rangle$ being the chiral condensate in the mean field limit

$$\langle\langle\bar{\psi}_i\psi_i\rangle\rangle = -2N_c \int_0^\Lambda \frac{d^3p}{(2\pi)^3} \frac{m_i}{E_{\mathbf{p}}} [1 - f_q - f_{\bar{q}}] \quad (4)$$

with $E_{\mathbf{p}} = \sqrt{\mathbf{p}^2 + m^2}$, Λ being the NJL cutoff, and the Fermi-Dirac distribution

$$\begin{aligned} f_q(\mathbf{p}, T, \mu) &= (\exp[(E_{\mathbf{p}} - \mu)/T] + 1)^{-1} \\ f_{\bar{q}}(\mathbf{p}, T, \mu) &= (\exp[(E_{\mathbf{p}} + \mu)/T] + 1)^{-1}. \end{aligned} \quad (5)$$

The NJL model is a non-renormalizable model which has to be regularized in the ultraviolet limit using a cutoff parameter Λ . The set of parameters for our calculations is displayed in Table I.

We construct the meson propagator as a series of q/\bar{q} polarization loops which give

$$\frac{-ig_{\pi q\bar{q}}^2}{k^2 - M^2} = \frac{2iG}{1 - 2G\Pi(k)}, \quad (6)$$

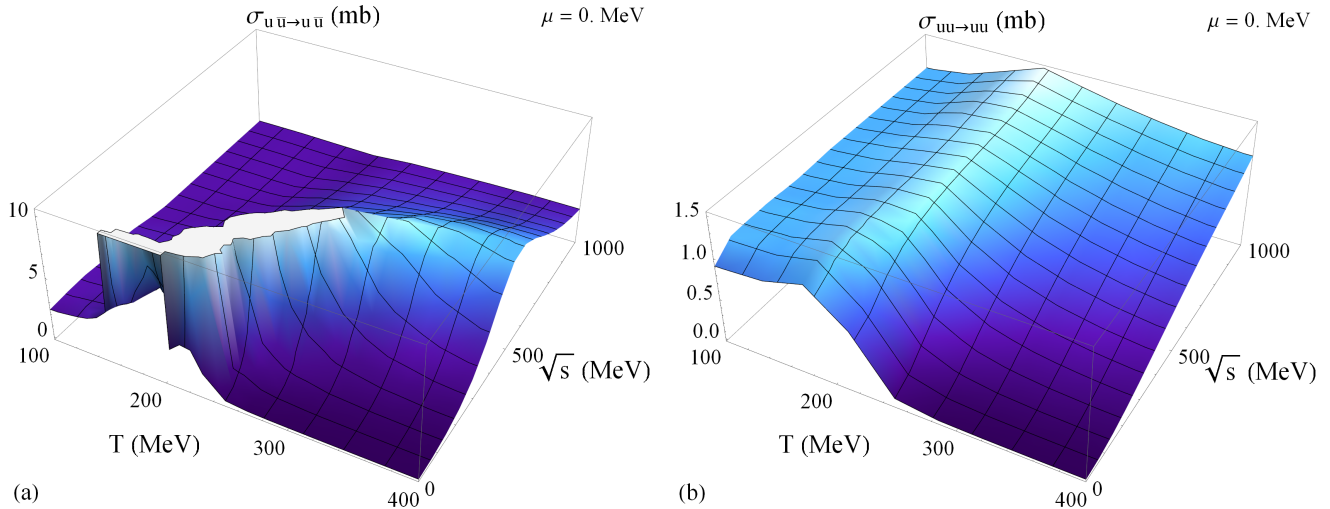


FIG. 3. Cross sections $u\bar{u} \rightarrow u\bar{u}$ (a) and $uu \rightarrow uu$ (b) as a function of (T, \sqrt{s}) in the NJL model.

with $\Pi(k)$ being the q/\bar{q} polarization loop (see [12]). The mass of the meson is obtained by solving the equation

$$1 - 2G\Pi(k)|_{k^2=M^2} = 0. \quad (7)$$

For our study we have a preferential interest in the partonic degrees of freedom and therefore we refer the reader to Ref. [11, 13] for further information about the basics on the NJL model.

Masses of quarks and pseudoscalar mesons from the NJL calculations are displayed in Fig. 1. At low temperatures T the spontaneous breaking of chiral symmetry generates an effective mass for the quarks. On the contrary, the pseudoscalar mesons show an increasing mass with increasing temperature. We can define a Mott temperature as that temperature when the mass of mesons is equal to the mass of the intrinsic quarks+antiquarks, i.e. $M = m_q + m_{\bar{q}}$.

It is also possible to compute these masses at finite chemical potential μ as shown in Fig. 2. For small temperature T and large chemical potential μ , the cross over transition between the hadronic and partonic phase turns to a first order phase transition in the NJL model [14, 15].

The Lagrangian (1) allows to compute cross sections using quark or meson exchange diagrams [17]. We can see in Fig. 3(a) that in the case of quark-antiquark scattering the resonant s -channel gives very large cross sections around the Mott temperature whereas the cross section for quark-quark scattering (Fig. 3(b)) stays roughly flat and is small. Note that different mesons have different Mott temperatures. We define for the rest of this study a critical temperature $T_c = T_{\text{Mott}} = 200$ MeV which is about the mean value of the different Mott temperatures in the NJL model.

Λ	$G\Lambda^2$	$K\Lambda^5$	m_{0q}	m_{0s}
602.3 MeV	1.835	12.36	5.5 MeV	140.7 MeV

TABLE I. Parameters for the NJL model from Ref. [16].

III. THE POLYAKOV-NAMBU-JONA-LASINIO MODEL

The NJL model assumes the gluon degrees of freedom to be integrated out and therefore confinement is not included in the model. However, gluons can be included on the level of a chiral-point coupling of quarks together with a static background field representing the Polyakov loop [18]. This Polyakov loop extended NJL model –denoted as PNJL– was developed by fitting lattice pure gauge data and considering additionally three flavors of quarks in Refs. [3, 19, 20]. The PNJL Lagrangian used in Ref. [19] is:

$$\begin{aligned} \mathcal{L}_{PNJL} = & \bar{\psi}(i\not{D} - m_0)\psi + \mathcal{U}(\phi, \bar{\phi}, T) + \mu \bar{\psi}\gamma_0\psi \\ & + G \sum_{a=0}^8 \left[(\bar{\psi}\lambda^a\psi)^2 + (\bar{\psi}i\gamma_5\lambda^a\psi)^2 \right] \\ & + K [\det\bar{\psi}(1 - \gamma_5)\psi + \det\bar{\psi}(1 + \gamma_5)\psi]. \end{aligned} \quad (8)$$

which differs from Eq. (1) by adding an external gauge field $D^\mu = \partial^\mu - iA^\mu$ with $A^\mu = \delta_0^\mu A^0$ (Polyakov gauge), in Euclidean notation $A^0 = -iA_4$, and by adding an effective potential \mathcal{U} which depends on the Polyakov loop ϕ :

$$\Phi(\vec{x}) = \frac{1}{N_c} \text{Tr}_c \langle \langle L(\vec{x}) \rangle \rangle, \quad (9)$$

where

$$L(\vec{x}) = \mathcal{P} \exp \left[i \int_0^\beta d\tau A_4(\vec{x}, \tau) \right]. \quad (10)$$

One can also extend this approach to finite baryon densities n_B by adding $\mu \bar{\psi}\gamma_0\psi \approx \mu \langle \langle \psi^\dagger \psi \rangle \rangle = -\mu n_B$ to the Lagrangian (8). Note, however, the Polyakov loop potential might vary additionally explicitly with μ .

Linking the Polyakov loop to the quark degrees of freedom then modifies the Fermi-Dirac distribution to

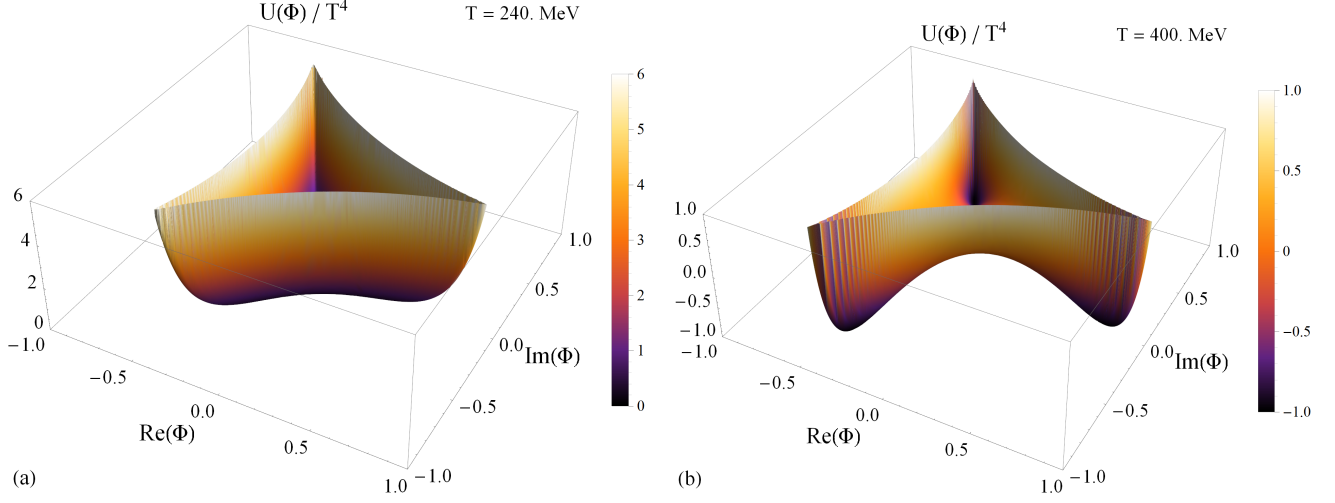


FIG. 4. Polyakov potential \mathcal{U} as a function of the real and imaginary part of the Polyakov loop ϕ for $T < T_c$ (a) and $T > T_c$ (b).

$$f_q \rightarrow f_q^\Phi(\mathbf{p}, T, \mu) = \frac{(\bar{\Phi} + 2\Phi e^{-(E_p - \mu)/T}) e^{-(E_p - \mu)/T} + e^{-3(E_p - \mu)/T}}{1 + 3(\bar{\Phi} + \Phi e^{-(E_p - \mu)/T}) e^{-(E_p - \mu)/T} + e^{-3(E_p - \mu)/T}}, \quad (11)$$

$$f_{\bar{q}} \rightarrow f_{\bar{q}}^\Phi(\mathbf{p}, T, \mu) = \frac{(\Phi + 2\bar{\Phi} e^{-(E_p + \mu)/T}) e^{-(E_p + \mu)/T} + e^{-3(E_p + \mu)/T}}{1 + 3(\Phi + \bar{\Phi} e^{-(E_p + \mu)/T}) e^{-(E_p + \mu)/T} + e^{-3(E_p + \mu)/T}}.$$

This distribution approaches the standard definition (Eq. (5)) for $\Phi \rightarrow 1$ in the deconfined phase. For $\Phi \rightarrow 0$, the quarks are supposed to be confined in neutral bound states and therefore the exponent in the Boltzmann distribution increases by a factor of three.

The static background field—firstly defined in Ref. [21], and then modified in [22]—is assumed to be

$$\frac{\mathcal{U}(\Phi, \bar{\Phi}, T)}{T^4} = -\frac{a(T)}{2} \bar{\Phi} \Phi + b(T) \log[1 - 6\bar{\Phi} \Phi + 4(\bar{\Phi}^3 + \Phi^3) + 3(\bar{\Phi} \Phi)^2], \quad (12)$$

where

$$a(T) = a_0 + a_1 \left(\frac{T_0}{T}\right) + a_2 \left(\frac{T_0}{T}\right)^2, \quad (13)$$

$$b(T) = b_3 \left(\frac{T_0}{T}\right)^3.$$

From pure gauge lattice data [23] one can extract the parameters which are depicted in Table II.

The quark masses as well as of Φ and $\bar{\Phi}$ are obtained by minimizing the grand canonical potential [19] for all these four degrees of freedom. For the masses one finds the same gap

a_0	a_1	a_2	b_3	T_0
3.51	-2.47	15.2	-1.75	270

TABLE II. Parameters for the effective potential in the pure gauge sector (Eq. (12)).

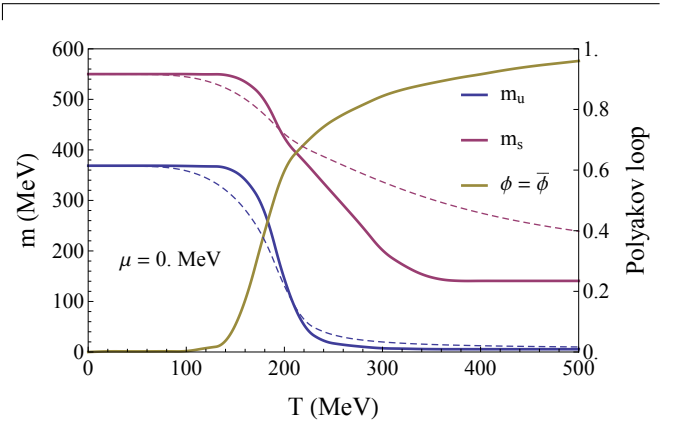


FIG. 5. Masses of quarks and Polyakov loop Φ as a function of T in the PNJL model (full lines) [19] and in the NJL model (dashed lines).

equation as Eq. (3) for NJL. Only the Fermi-Dirac distributions are replaced by Eq. (11):

$$\langle\langle \bar{\psi} \psi \rangle\rangle = -2N_c \int_0^\Lambda \frac{d^3 p}{(2\pi)^3} \frac{m}{E_p} [1 - f_q^\Phi - f_{\bar{q}}^\Phi]. \quad (14)$$

The result for the masses and the Polyakov loop are displayed in Fig. 5. For the comparison with the results of the NJL model the gauge temperature T_0 has been modified to $T_0 = 210$ MeV. We see immediately the effect of the Polyakov loop on the phase transition: close to the transition the change of mass is faster for PNJL than NJL. Nevertheless, for $T \rightarrow 0$ or ∞ one recovers the same mass limit for the NJL and the PNJL models.

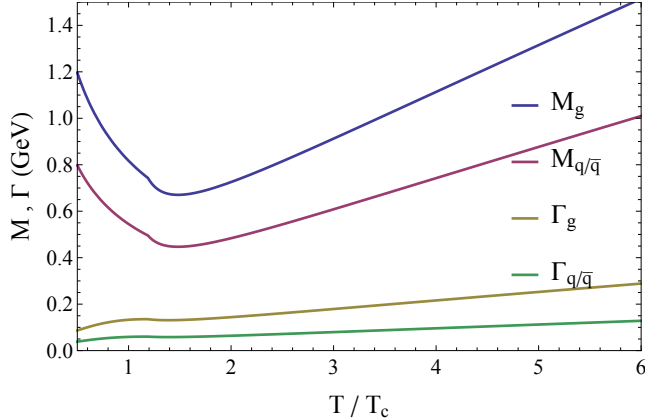


FIG. 6. Masses and widths of quarks and gluons as a function of T/T_c in the DQPM [26].

IV. THE DYNAMICAL QUASI-PARTICLE MODEL

The dynamical quasi-particle model [4, 5] describes QCD properties in terms of “resummed” single-particle Green’s functions (in the sense of a two-particle irreducible (2 PI) approach). The parameters of the model are fitted in order to reproduce the equation of state from Ref. [24] above temperatures of 140 MeV.

This approach doesn’t involve an effective lagrangian since the strong coupling and propagators are assumed to represent “resummed” quantities. The 2 PI framework then guarantees a consistent description of systems in-and out-of equilibrium on the basis of Kadanoff-Baym equations [25]. The resummed propagators are specified by complex selfenergies that are temperature dependent. Whereas the real part of the selfenergy describes a dynamically generated mass the imaginary part provides the interaction width of partons [8]; the mass and the width are linked in turn to the coupling constant $g^2(T)$ for strongly interacting matter which is found to be enhanced in the infrared (or low temperature).

The running coupling constant $g^2(T)$ for partons is approximated (for $T > T_c$, $\mu_q = 0$) by

$$g^2(T/T_c) = \frac{48\pi^2}{(11N_c - 2N_f)\ln[\lambda^2(T/T_c - T_s/T_c)^2]}, \quad (15)$$

where the parameters $\lambda = 2.42$ and $T_s/T_c = 0.56$ have been extracted from a fit to the lattice data for purely gluonic systems ($N_f = 0$). In Eq. (15), $N_c = 3$ stands for the number of colors, T_c is the critical temperature ($= 158$ MeV), while N_f denotes the number of flavors.

The functional forms for the dynamical masses of quasi-particles (gluons and quarks) are chosen so that they become identical to the perturbative thermal masses in the asymptotic high-temperature regime, i.e., for gluons

$$M_g^2(T, \mu_q) = \frac{g^2}{6} \left(\left(N_c + \frac{N_f}{2} \right) T^2 + \frac{N_c}{2} \sum_q \frac{\mu_q^2}{\pi^2} \right), \quad (16)$$

and for quarks (antiquarks)

$$M_{q/\bar{q}}^2(T, \mu_q) = \frac{N_c^2 - 1}{8N_c} g^2 \left(T^2 + \sum_q \frac{\mu_q^2}{\pi^2} \right), \quad (17)$$

but the running coupling $g^2(T)$ is considered as the resummed coupling of Eq. (15). The effective degrees of freedom (quarks, antiquarks and gluons) in the DQPM have finite widths, which for $\mu_q = 0$ read

$$\begin{aligned} \Gamma_g(T) &= \frac{1}{3} N_c \frac{g^2 T}{8\pi} \ln \left(\frac{2c}{g^2} + 1 \right), \\ \Gamma_{q/\bar{q}}(T) &= \frac{1}{3} \frac{N_c^2 - 1}{2N_c} \frac{g^2 T}{8\pi} \ln \left(\frac{2c}{g^2} + 1 \right), \end{aligned} \quad (18)$$

where the parameter $c = 14.4$ is related to a magnetic cut-off.

For fitting the equations of state of lattice QCD (from Ref. [24]) for 3 flavors the coupling constant has been modified around T_c and below and reads:

$$g^2(T/T_c) \rightarrow g^2(T^*/T_c) \left(\frac{T^*}{T} \right)^\gamma, \quad (19)$$

where $T^* = 1.19T_c$ and $\gamma = 3.1$. The masses and widths used in the DQPM are displayed in Fig. 6 as a function of T/T_c .

Due to the finite imaginary parts of the selfenergies the parton spectral functions, i.e. the imaginary parts of the propagators, are no longer δ -functions in the invariant mass squared but have a Breit-Wigner form

$$\rho(\omega, \mathbf{p}) = \frac{\Gamma}{E} \left(\frac{1}{(\omega - E)^2 + \Gamma^2} - \frac{1}{(\omega + E)^2 + \Gamma^2} \right) \quad (20)$$

with the notation $E^2(\mathbf{p}^2) = \mathbf{p}^2 + M^2 - \Gamma^2$, for quarks, antiquarks and gluons. The spectral function (20) is antisymmetric in ω and normalized as

$$\int_{-\infty}^{\infty} \frac{d\omega}{2\pi} \omega \rho(\omega, \mathbf{p}) = \int_0^{\infty} \frac{d\omega}{2\pi} 2\omega \rho(\omega, \mathbf{p}) = 1. \quad (21)$$

The equations (15) to (21) specify the DQPM (and its few parameters); all further quantities discussed in this study then are fully defined and do not require any further assumptions. Although the free parameters of the DQPM are fitted to the LQCD equation of state in equilibrium its results for the various transport coefficients (investigated in this article) are a direct consequence within the model without incorporating any additional parameter.

V. EQUATIONS OF STATE

In order to compute the equation of state of strongly interacting matter, we use thermal distribution functions for partons, i.e. Eq. (5) for quarks in the NJL and DQPM approach and Eq. (11) for quarks in the PNJL model. For the gluons in the DQPM we use the Bose-Einstein distribution:

$$f_g(\mathbf{p}, T) = (\exp[E_{\mathbf{p}}/T] - 1)^{-1}, \quad (22)$$

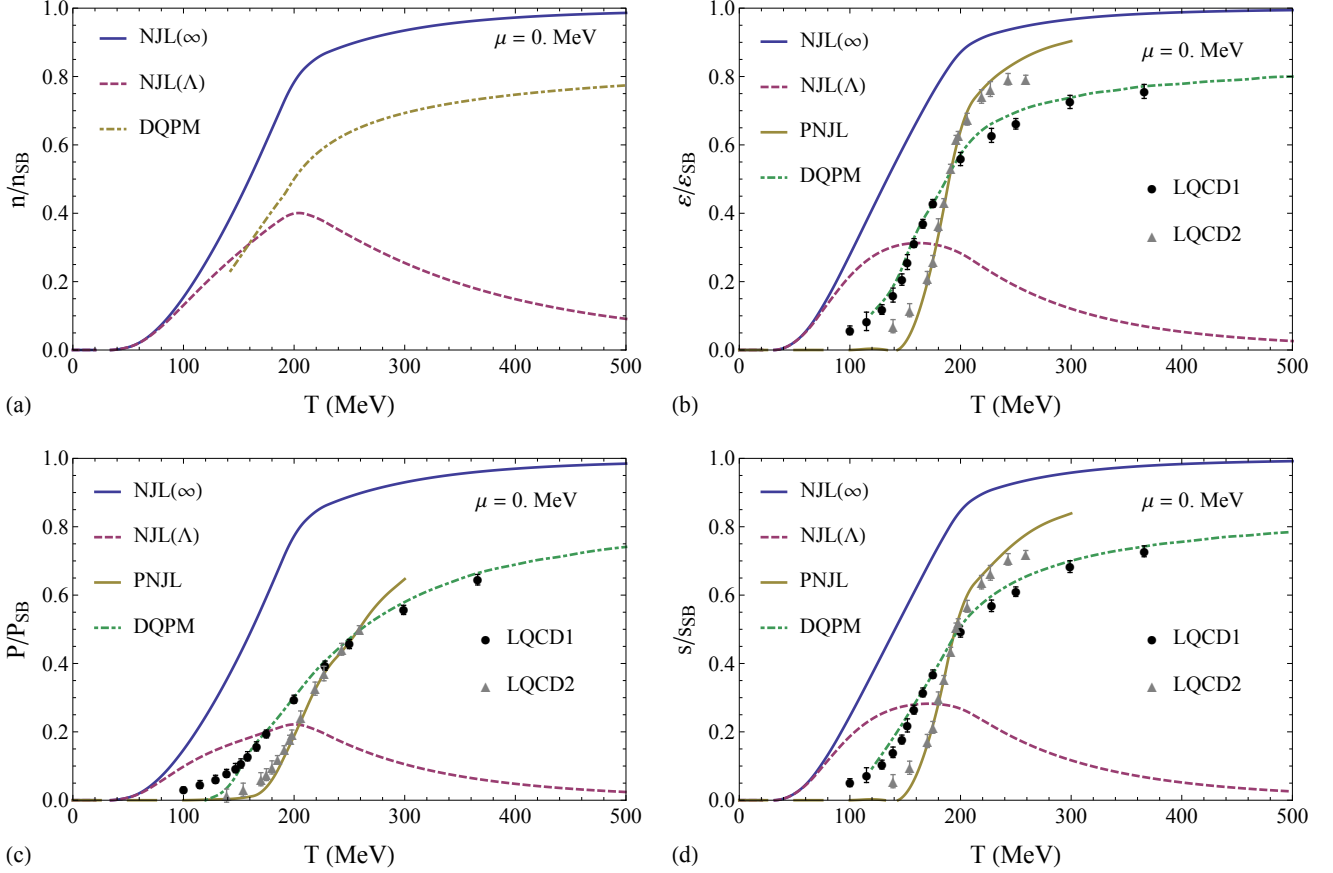


FIG. 7. Particle density n (a), energy density ε (b), pressure density P (c) and entropy density s (d) as a function of temperature T from different models compared to LQCD1 data from Ref. [27] and LQCD2 data from [28]. The PNJL results have been taken from Ref. [20].

with $E(\mathbf{p}, T, \mu) = \sqrt{\mathbf{p}^2 + m_g^2}$ and $m_g(T, \mu)$ being an effective mass for gluons. We note that the temperature and density dependence of the different quark masses $m_q(T, \mu)$ are rather different in the DQPM as compared to the (P)NJL model.

We compute the particle density n , energy density ε , pressure P , and entropy density s (cf. Fig. 7) in the NJL model as a function of temperature T using the relations based on the definition of the stress-energy tensor $T^{\mu\nu}$ for non-interacting particles:

$$n(T, \mu) = g_g \int_0^\infty \frac{d^3 p}{(2\pi)^3} f_g + \frac{g_q}{6} \int_0^\infty \frac{d^3 p}{(2\pi)^3} \left[\sum_q^{u,d,s} f_q + \sum_{\bar{q}}^{\bar{u},\bar{d},\bar{s}} f_{\bar{q}} \right], \quad (23)$$

$$P(T, \mu) = g_g \int_0^\infty \frac{d^3 p}{(2\pi)^3} f_g \frac{\mathbf{p}^2}{3E_g} + \frac{g_q}{6} \int_0^\infty \frac{d^3 p}{(2\pi)^3} \left[\sum_q^{u,d,s} f_q + \sum_{\bar{q}}^{\bar{u},\bar{d},\bar{s}} f_{\bar{q}} \right] \frac{\mathbf{p}^2}{3E_q}, \quad (24)$$

$$\varepsilon(T, \mu) = g_g \int_0^\infty \frac{d^3 p}{(2\pi)^3} f_g E_g + \frac{g_q}{6} \int_0^\infty \frac{d^3 p}{(2\pi)^3} \left[\sum_q^{u,d,s} f_q + \sum_{\bar{q}}^{\bar{u},\bar{d},\bar{s}} f_{\bar{q}} \right] E_q, \quad (25)$$

$$s(T, \mu) = \frac{\varepsilon(T, \mu) + P(T, \mu) - \mu n_B(T, \mu)}{T}, \quad (26)$$

with the baryonic density

$$n_B(T, \mu) = \frac{g_q}{6} \int_0^\infty \frac{d^3 p}{(2\pi)^3} \left[\sum_q^{u,d,s} f_q - \sum_{\bar{q}}^{\bar{u},\bar{d},\bar{s}} f_{\bar{q}} \right], \quad (27)$$

and the degeneracy factors

$$g_g = \text{polarization } [0, 1] \times (N_c^2 - 1) = 16, \quad (28)$$

$$g_q = \text{spin } [+1/2, -1/2] \times \text{parity } [q, \bar{q}] \times N_c N_f = 36.$$

The case of the (P)NJL model is treated differently, first of all because there are no gluons in the model but also because the model is an effective approach and therefore it involves an ultraviolet cut-off Λ on the 3-momentum for taking into

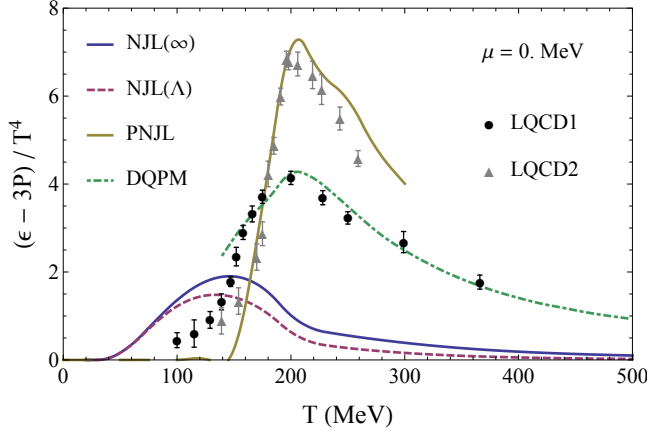


FIG. 8. Trace anomaly $(\epsilon - 3P)/T^4$ as a function of T from different models compared to LQCD data 1 from Ref. [27] and LQCD data 2 from [28]. The PNJL results have been taken from Ref. [20].

account the vacuum energy density of the quark condensate $\langle\langle\bar{q}q\rangle\rangle$ [11]. When keeping this cut-off in the calculation of the equations of state, we cannot reach the Stephan-Boltzmann limit (see Fig. 7). For the following results we don't use this limit considering a realistic medium where the momenta of the partons are thermally distributed and the cut-off is removed.

The Stephan-Boltzmann limit is defined by

$$n_{SB}(T) = \left(g_g + \frac{3}{4}g_q\right) \frac{\zeta(3)}{\pi^2} T^3 \quad (29)$$

with $\zeta(3) \simeq 1.202$ for the particle density and

$$P_{SB}(T, \mu) = \frac{g_g}{72} 0.8\pi^2 T^4 + \frac{g_q}{72} \left(0.7\pi^2 T^4 + 2T^2 \mu_q^2 + \frac{\mu_q^4}{\pi^2}\right) \quad (30)$$

for the pressure density, in which the first term stands for the gluon degrees-of-freedom and the second for that of the quarks. In the SB limit we have the relations:

$$\begin{aligned} \epsilon_{SB}(T, \mu) &= 3P_{SB}(T, \mu), \\ s_{SB}(T, \mu) &= 4P_{SB}(T, \mu)T. \end{aligned} \quad (31)$$

In Fig. 7 the SB limit is different for the NJL model and for PNJL/LQCD due to the lack of the gluon degrees of freedom. We recall that the results of the Polyakov-NJL model differ from the NJL results due to the explicit gluon potential \mathcal{U} [20].

The critical temperature T_c is also different between the NJL, PNJL and LQCD. In the NJL model the definition of T_c from the equation of state is different from the Mott temperatures for the different processes (see above). For convenience we choose an intermediate value $T_c \simeq 200$ MeV. For the DQPM this value is taken from the Wuppertal-Budapest LQCD Collaboration [24, 29] as $T_c \simeq 158$ MeV, and for the PNJL from the HotQCD LQCD Collaboration [28] as $T_c \simeq 185$ MeV. Note that the different critical temperatures from the LQCD Collaborations are due to different discretizations of the action and different fermion masses, respectively.

The approach for calculating the equation of state in the DQPM is different but thermodynamically consistent. One here starts from the evaluation of the entropy density s within the quasiparticle approach [4, 7] which depends on the complex propagators and complex self energies of the degrees of freedom as well as thermal Bose or Fermi distributions. Note that this entropy stands for an interacting system. Then using the thermodynamic relation

$$s(T) = \left(\frac{\partial P(T)}{\partial T}\right)_\mu \quad (32)$$

(for a fixed chemical potential μ) one obtains the pressure P by integration of $s(T)$ over T while the energy density ϵ is gained using Eq. (26). A self-consistent check is to compare the result with Eq. (25). In the DQPM one has to include the off-shellness of the degrees of freedom by replacing

$$f(E_{\mathbf{p}}) \rightarrow \int_0^\infty \frac{d\omega}{2\pi} f(\omega) \rho(\omega, \mathbf{p}) 2\omega \quad (33)$$

with the spectral function $\rho(\omega)$ (Eq. (20)) and then integrating over ω additionally.

We also note that the grand canonical potential Ω is used in the (P)NJL model to compute the pressure using the relation $P(T, \mu) = -\Omega(T, \mu)$.

In Fig. 8 we display the interaction measure –known in LQCD as the trace anomaly– in comparison with LQCD and find again the NJL model not to be in good agreement with lattice data from Ref. [27, 28]. Note that the PNJL [20] and DQPM calculations agree well with the LQCD data, however, both have been adjusted to different LQCD results, i.e. either to those from Ref. [27] (DQPM) or from Ref. [28] (PNJL). We recall that the gluon pressure is taken into account in the PNJL model [3, 20].

The derivatives of the previous densities provide further interesting quantities. For instance we can compute the specific

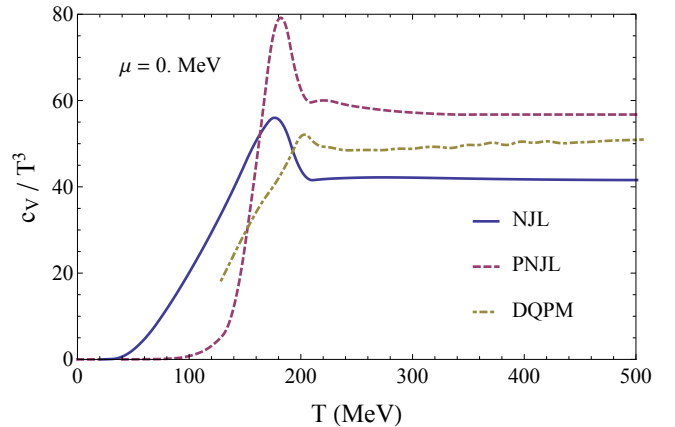


FIG. 9. Specific heat c_V as a function of T in the NJL, DQPM and in the PNJL (taken from Ref. [30]).

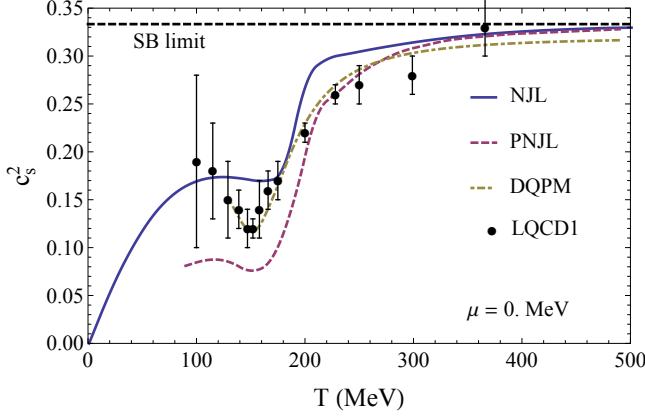


FIG. 10. Speed of sound squared c_s^2 for the NJL model, for the PNJL from Ref. [30], and the DQPM as a function of T compared to LQCD data from Ref. [24].

heat c_V and the speed of sound c_s^2 as

$$c_V = T \left(\frac{\partial s}{\partial T} \right)_V = T \left(\chi_{TT} - \frac{\chi_{\mu T}^2}{\chi_{\mu\mu}} \right) \quad (34)$$

and

$$c_s^2 = \left(\frac{\partial P}{\partial \varepsilon} \right)_{n_B} = \frac{s\chi_{\mu\mu} - n_B\chi_{\mu T}}{c_V\chi_{\mu\mu}} \quad (35)$$

with the susceptibilities $\chi_{xy} = \partial^2 P / \partial x \partial y$.

Fig. 9 shows the scaled specific heat c_V/T^3 which reaches a limit above T_c . This limit is not the same for the different model calculations because the PNJL model and the DQPM include gluon degrees of freedom in the pressure which changes the SB limit and the specific heat accordingly. Note that the parametrization of the PNJL model from Ref. [30] is fitted to different IQCD data than Ref. [19].

In Fig. 10 we display the speed of sound squared $c_s^2(T)$ (from Ref. [24]) as a function of T . c_s^2 passes through a local minimum around the critical temperature and then reaches the SB limit ($= 1/3$) at high temperature T . This minimum indicates a fast change in the masses of partons in the (P)NJL model (e.g. quarks) as well as the DQPM (cf. Fig. 6).

VI. INTEGRATED CROSS SECTIONS

The first step before computing transport coefficients in the NJL model is to integrate the elastic cross sections $\sigma(T, \mu, s)$ over the invariant energy squared s taking into account all possible kinematic reactions for a given thermodynamical medium in equilibrium for fixed (T, μ) . The integration is done using [31]:

$$\sigma(T, \mu) = \int_{\text{Th}}^{\infty} ds \sigma(T, \mu, s) L(T, \mu, s), \quad (36)$$

with the threshold $\text{Th} = \max((m_1 + m_2)^2, (m_3 + m_4)^2)$ (which depends on (T, μ)) and L being the probability of yielding a

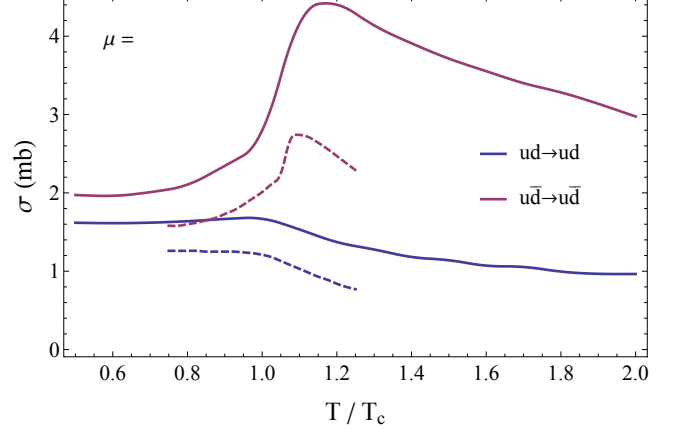


FIG. 11. Cross sections as a function of T in the NJL model (dashed lines from Ref. [1]).

$q\bar{q}$ (qq) pair with the energy \sqrt{s} in the medium (T, μ) :

$$L(T, \mu, s) = 2\sqrt{s} C(T, \mu) p_{\text{cm}}(s) v_{\text{rel}}(s) f_q \left(\frac{\sqrt{s}}{2} - \mu \right) f_{\bar{q}}(s) \left(\frac{\sqrt{s}}{2} + (-)\mu \right) \quad (37)$$

with the center-of-mass momentum

$$p_{\text{cm}}(s) = \frac{\sqrt{(s - (m_1 + m_2)^2)(s - (m_1 - m_2)^2)}}{2\sqrt{s}}, \quad (38)$$

the relative velocity (in the center of mass)

$$v_{\text{rel}}(s) = \frac{\sqrt{(p_1 p_2)^2 - (m_1 m_2)^2}}{E_1 E_2} = \frac{p_{\text{cm}}(s)\sqrt{s}}{E_1 E_2} = \frac{p_{\text{cm}}}{E_1} + \frac{p_{\text{cm}}}{E_2}, \quad (39)$$

while C is a normalization factor fixed by

$$C^{-1}(T, \mu) = \int_{\text{Th}}^{\infty} ds L(T, \mu, s). \quad (40)$$

The factor $2\sqrt{s}p_{\text{cm}}(s)v_{\text{rel}}(s)$ represents the flux of the colliding particles. Similar calculations can be performed for cross sections with massive gluons by including the Bose-Einstein distribution in Eq. (37).

Now we can integrate the 11 different elastic NJL cross sections [1] over s :

- 4 $qq \rightarrow qq$ cross sections,
- 4 $q\bar{q} \rightarrow q\bar{q}$ cross sections,
- 3 $q\bar{q} \rightarrow q'\bar{q}'$ cross sections.

We show the results for the channels $ud \rightarrow ud$ and $u\bar{d} \rightarrow u\bar{d}$ in Fig. 11 which are in good agreement with the previous calculations from Ref. [1]. We can see that while the shape of the cross section is similar (e.g. flat qq and peaked $q\bar{q}$ cross sections) the maximum is different.

For the DQPM we do not need the explicit cross sections since the inherent quasiparticle width $\Gamma(T)$ directly provides the total interaction rate.

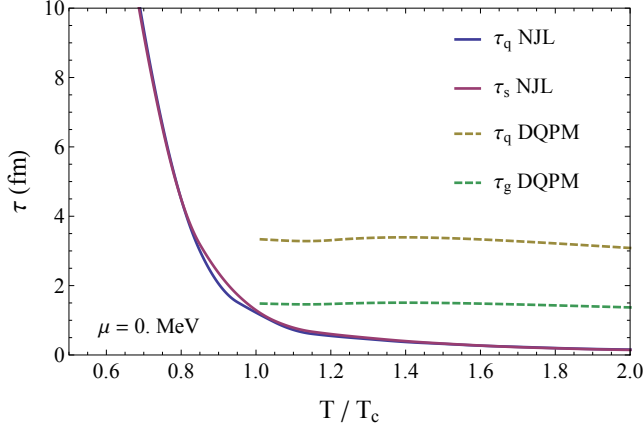


FIG. 12. Relaxation times τ as a function of T/T_c from the NJL model and the DQPM.

VII. RELAXATION TIMES

By means of the integrated cross sections we can compute the relaxation time τ of particles within the NJL model. This quantity relates to the mean-free-path between two elastic collisions as [31]:

$$\tau_i^{-1}(T, \mu) = \sum_j n_j(T, \mu) \sigma_{ij}(T, \mu), \quad (41)$$

with $j = u, d, s, \bar{u}, \bar{d}, \bar{s}, g$, and the densities

$$n_j(T, \mu) = \int_0^\infty \frac{d^3 p}{(2\pi)^3 (\hbar c)^3} f_j, \quad (42)$$

In the DQPM approach one can directly use the flavor-blind reaction rates based on the particle width (18) [26]:

$$\tau_q^{-1}(T) = \Gamma_q(T) \text{ and } \tau_g^{-1}(T) = \Gamma_g(T). \quad (43)$$

For example the relaxation time in the NJL model for a u quark (knowing that we have isospin symmetry for u and d quarks and no gluons) reads:

$$\begin{aligned} \tau_u^{-1} = & n_u (\sigma_{uu \rightarrow uu} + \sigma_{ud \rightarrow ud}) + n_{\bar{u}} (\sigma_{u\bar{u} \rightarrow u\bar{u}} \\ & + \sigma_{u\bar{d} \rightarrow u\bar{d}} + \sigma_{u\bar{u} \rightarrow d\bar{d}} + \sigma_{u\bar{u} \rightarrow s\bar{s}}) \\ & + n_s (\sigma_{us \rightarrow us} + n_{\bar{s}} \sigma_{u\bar{s} \rightarrow u\bar{s}}). \end{aligned} \quad (44)$$

We note that elastic processes involving chemical equilibration are included in the computation of the relaxation time [32].

Fig. 12 shows the relaxation time for the NJL model for u and s quarks as well as the relaxation time for quarks (flavor-blind) and gluons for the DQPM as a function of the temperature T/T_c , with $T_c = 200$ MeV for the NJL model and $T_c = 158$ MeV for the DQPM. We can evaluate –in terms of powers of T – the behavior of this relaxation time for the NJL model [33]:

$$T < T_c : \begin{cases} n \propto e^{-m/T} \\ \sigma \propto \text{const.} \end{cases} \Rightarrow \tau \propto e^{-T} \quad (45)$$

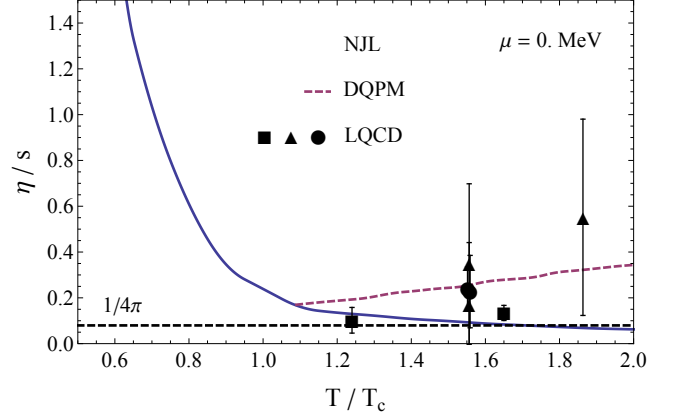


FIG. 13. Shear viscosity to entropy density ratio η/s as a function of T/T_c compared to the LQCD data points from Ref. [34] (square), [35] (triangle) and [36] (circle) and the result from the DQPM.

and

$$T > T_c : \begin{cases} n \propto T^3 \\ \sigma \propto T^{-2} \end{cases} \Rightarrow \tau \propto T^{-1} \quad (46)$$

The density is proportional to T^3 for large temperature where $m \ll T$ in the NJL model whereas the fast increase of the mass below T_c gives an exponential decrease. The integrated cross sections are roughly constant up to T_c and then are proportional to $1/T^2$ above T_c .

Once one has the relaxation time for the different quark species, it is straight forward to compute all transport coefficients (viscosities and conductivities) in the relaxation time approximation [32]. Obviously all results are strongly T -dependent and a systematic study on the T dependence is mandatory.

VIII. SHEAR VISCOSITY

The shear viscosity η is related to the transverse motion of a particle during the expansion of a plasma. The calculation of this quantity is very important for the evaluation of physical observables such as the elliptic flow v_2 . It is defined in the dilute gas approximation for interacting particles as [39]:

$$\begin{aligned} \eta(T, \mu) = & \frac{1}{15T} g_g \int_0^\infty \frac{d^3 p}{(2\pi)^3} \tau_g f_g \frac{\mathbf{p}^4}{E_g^2} \\ & + \frac{1}{15T} \frac{g_q}{6} \int_0^\infty \frac{d^3 p}{(2\pi)^3} \left[\sum_q^{u,d,s} \tau_q f_q + \sum_{\bar{q}}^{\bar{u},\bar{d},\bar{s}} \tau_{\bar{q}} f_{\bar{q}} \right] \frac{\mathbf{p}^4}{E_q^2}. \end{aligned} \quad (47)$$

Another approach to compute the shear viscosity is to use the stress-energy tensor and the Green-Kubo formula to extract the viscosity [26, 40]. We don't discuss this method in the present study since explicit comparisons of both methods demonstrate that both solutions are rather close (at least in case of approximately isotropic scattering) [26, 40].

We note that in Ref. [32] the shear and bulk viscosities have been also calculated by restricting to elastic interactions. Their

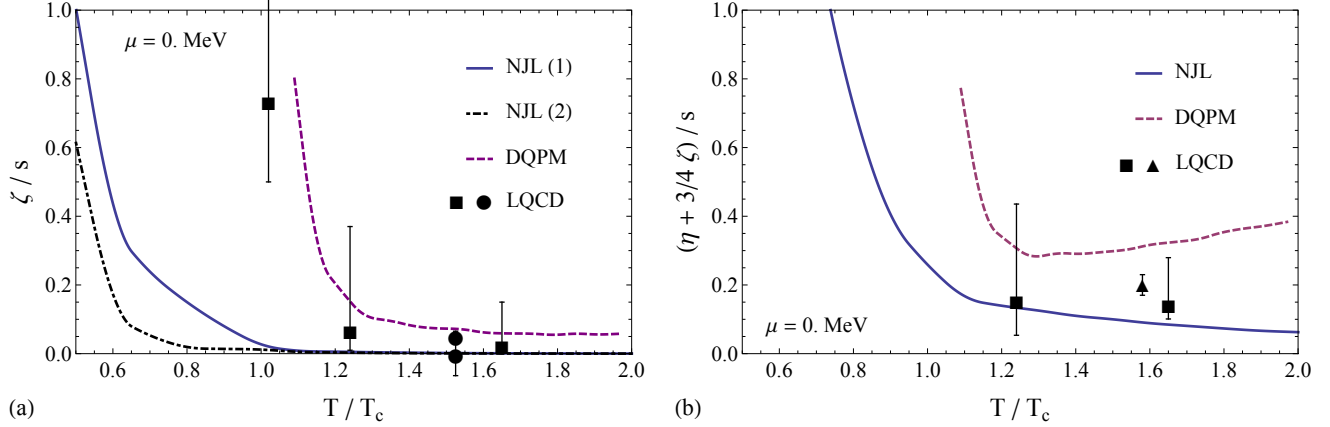


FIG. 14. Bulk viscosity to entropy density ratio ζ/s (a) compared to the LQCD data points from Ref. [37] (square) and [36] (circle), and specific sound channel (b) compared to the LQCD data points from Ref. [36, 37] (square) and [38] (triangle) as a function of T/T_c . For the NJL model, the bulk viscosity to entropy density ratio is computed with the method from Ref. [39] (1) as well as with the that from Ref. [32] (2). The results from the DQPM are shown by dashed lines.

result for the shear viscosity differs from ours only by a Pauli blocking factor $(1 - f)$ which is ≈ 1 for the temperatures of interest. Then the definition of the shear viscosity from Ref. [39] and [32] coincide.

We find that the shear viscosity over entropy density ratio $\eta/s(T)$ shows a temperature dependence close to that of the relaxation time $\tau(T)$ in the NJL model. That implies that for $\tau \propto T^{-1}$ for high temperatures one obtains a similar behavior for η/s in the NJL model. The order of magnitude of the NJL cross sections finally give a ratio η/s which is in good agreement with lattice QCD data from $1.2 T_c$ up to $1.5 T_c$. Nevertheless, the T^{-1} behavior of the viscosity in the NJL implies to go beyond the Kovtun-Son-Starinets (KSS) bound [41]:

$$\left(\frac{\eta}{s}\right)_{\text{KSS}} = \frac{1}{4\pi}, \quad (48)$$

$$\begin{aligned} \zeta(T, \mu) = & \frac{1}{9T} g_g \int_0^\infty \frac{d^3 p}{(2\pi)^3} \tau_g f_g \frac{1}{E_g^2} \left[\mathbf{p}^2 - 3c_s^2 \left(E_g^2 - T^2 \frac{dm_g^2}{dT^2} \right) \right]^2 \\ & + \frac{1}{9T} \frac{g_q}{6} \int_0^\infty \frac{d^3 p}{(2\pi)^3} \left[\sum_q^{u,d,s} \tau_q f_q + \sum_{\bar{q}}^{\bar{u},\bar{d},\bar{s}} \tau_q f_{\bar{q}} \right] \frac{1}{E_q^2} \left[\mathbf{p}^2 - 3c_s^2 \left(E_q^2 - T^2 \frac{dm_q^2}{dT^2} \right) \right]^2. \end{aligned} \quad (49)$$

This definition is different from Ref. [32], even if the same contributions appear (i.e. the mass derivative $\partial m/\partial T$, the energy E , the temperature T , and the speed of sound squared c_s^2). For convenience, we have performed calculation in both approaches in order to get some idea about the differences in results.

The main difference between the RTA approach of Ref. [39] and [32] is the definition of the perturbation in the stress-energy tensor $\Delta T^{\mu\nu}$. The RTA approach of Ref. [39] is based on kinetic theory and allows for both elastic and inelas-

tic scattering (with detailed balance) of an arbitrary number of species, and finally the most important: the viscosities and the equation of state are mutually consistent (the same interactions are used to compute them).

We recall again that the DQPM results agree quite well with LQCD data and give an increasing ratio η/s with temperature and approach the pQCD limit at high T as already discussed in Ref. [26].

IX. BULK VISCOSITY

The bulk viscosity defined in Ref. [39] reads in the relaxation time approximation (RTA)

tic scattering (with detailed balance) of an arbitrary number of species, and finally the most important: the viscosities and the equation of state are mutually consistent (the same interactions are used to compute them).

The bulk viscosity (divided by the entropy density s) from the NJL model is displayed in Fig. 14(a) and shows a very different temperature dependence than η/s . Indeed, for high temperatures we find the limit $\zeta/s \rightarrow 0$. Moreover, the behavior around T_c shows a peak in LQCD as well as in the DQPM. This peak is not seen in the NJL model (or shifted to much

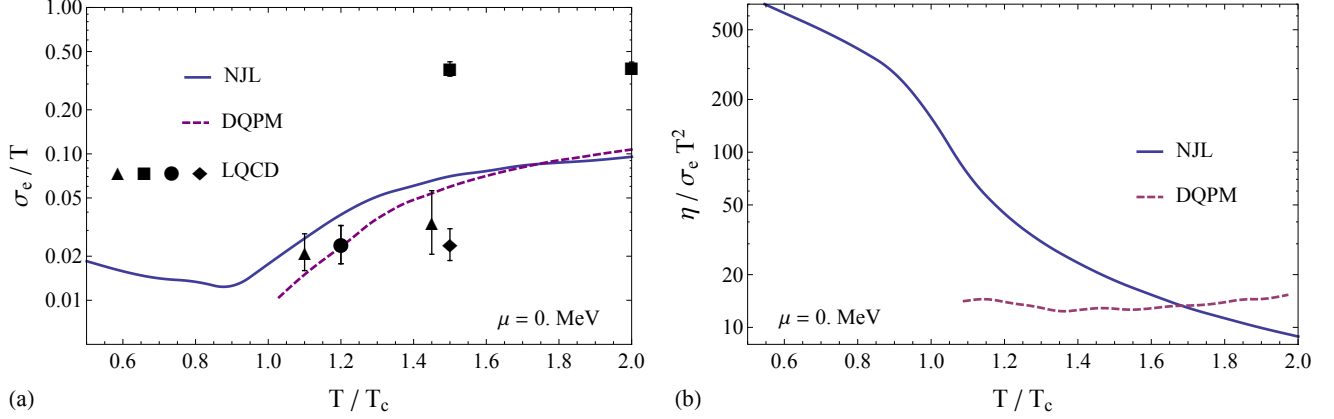


FIG. 15. The electric conductivity over T (a) compared to the LQCD data points from Ref. [42] (triangle), [43] (diamond), [44] (square) and [45] (circle) and the results from the DQPM (dashed lines); (b) electrical conductivity to shear viscosity ratio σ_e/η (b) as a function of T/T_c .

lower temperatures). This can be easily explained by the fact that the masses of the degrees of freedom play an important role for the bulk viscosity and the NJL masses do not change sufficiently fast in temperature around T_c to achieve a good agreement with LQCD or the DQPM. When replacing the NJL masses by PNJL masses this does not change the results in this case very much because one has to change the critical temperature as well, and therefore the fast increase of ζ/s close to T_c cannot be reproduced by any NJL-like model.

In the Fig. 14(b) we also display the specific sound channel $(\eta + 3/4\zeta)/s$ which is dominated by η/s in the NJL model and provides reasonable results for $T_c < T < 1.7T_c$ in comparison to LQCD.

X. ELECTRIC CONDUCTIVITY

The electric conductivity for charged particles –known as the Drude-Lorentz conductivity for a classical gas– is defined as [46, 47]:

$$\sigma_e(T, \mu) = \sum_q \frac{e_q^2 n_q(T, \mu) \tau_q(T, \mu)}{m_q(T, \mu)}, \quad (50)$$

with $q = u, d, s, \bar{u}, \bar{d}, \bar{s}$, and the electric charge of quarks:

$$e_q^2 = \frac{4\pi}{137} q^2, \quad (51)$$

with $q = +2/3$ or $-1/3$ denoting the quark electric charges fraction.

Fig. 15(a) shows that for the DQPM as well as the NJL model the dimensionless ratio of the electric conductivity over T behaves approximately linearly in T for $T \geq T_c$ up to about $2 T_c$ [47]. Both results are in a reasonable agreement with the present lattice QCD results although there is quite some uncertainty in the LQCD extrapolations.

In Fig. 15(b) we, furthermore, show the dimensionless ratio $\eta/\sigma_e T^2$ which is independent on the relaxation time τ . This ratio is roughly constant in the DQPM for $T_c < T < 2T_c$, however, drops rapidly in the NJL model with temperature T .

XI. HEAT CONDUCTIVITY

The heat conductivity κ is another quantity of interest that describes the heat flow in interacting systems [48, 49] and only recently has regained interest in the context of relativistic heavy-ion collisions [50, 51].

The heat conductivity for charged particles is defined using the specific heat c_V and the relaxation time [52]:

$$\kappa(T, \mu) = \frac{1}{3} v_{\text{rel}} c_V(T, \mu) \sum_f \tau_f(T, \mu), \quad (52)$$

with $f = u, d, s, \bar{u}, \bar{d}, \bar{s}$. For our purpose we assume that $v_{\text{rel}} \simeq 1$ in the NJL model because the masses of quarks decrease whereas the mean momentum increases with temperature T . Since all quantities entering in Eq. (52) have been specified before for the NJL model and the DQPM we directly step on with the actual results.

Fig. 16(a) displays the dimensionless quantity κ/T^2 for both models. Whereas the DQPM shows a slightly rising ratio for $T_c < T < 2T_c$ the NJL model predicts a rapid decrease with T for $T > T_c$.

In Fig. 16(b) we show the results of both models for the dimensionless ratio $\kappa/\sigma_e T$ which no longer depends on the relaxation time τ . For $T > T_c$ the results differ by more than an order of magnitude. Unfortunately, there are no lattice QCD results that might specify the quality of the predictions from both models.

XII. CONCLUSION

In this study we have calculated thermodynamic properties of the NJL model for three flavors (u, d, s) such as the energy density, entropy density, pressure, sound velocity, specific heat etc. as a function of temperature T up to a few times the critical temperature T_c . Furthermore, we have calculated the shear η and bulk ζ viscosity as well as the electric σ_e and heat conductivity κ as a function of T and compared to corresponding results from the DQPM, from the PNJL model and lattice QCD results when available.

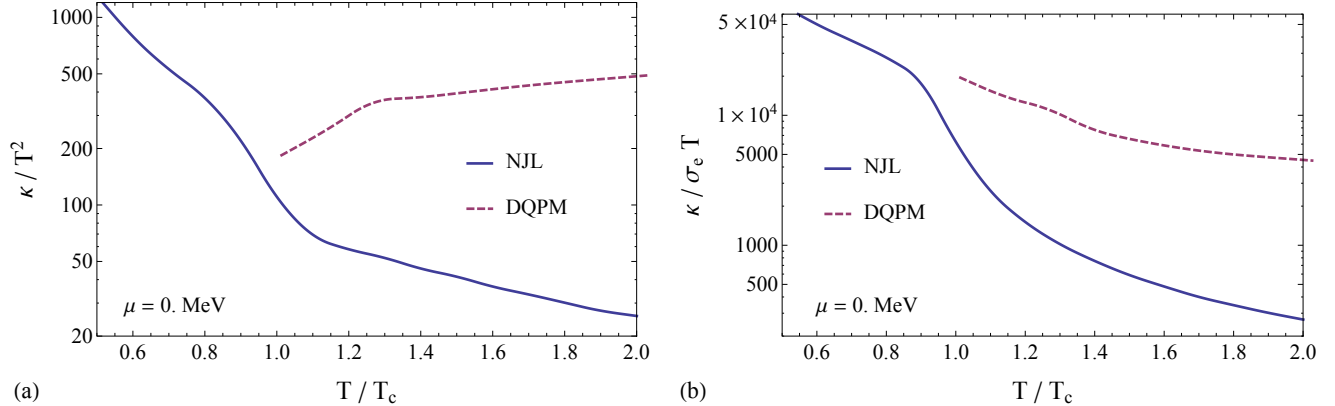


FIG. 16. Heat conductivity over T^2 (a) and heat to electrical conductivity $\kappa/\sigma_e T$ (b) as a function of T/T_c in the NJL model and the DQPM.

We recall that the NJL Lagrangian parameters (as well as a momentum cutoff) are essentially fixed at $T = 0$ by the pion (kaon) decay constant and pion (kaon) mass whereas the PNJL model is improved especially around the critical temperature T_c by adding a Polyakov loop potential (fitted to reproduce specific lattice data of the HOT-QCD Collaboration). Both models have in common that the Lagrangians share the symmetries of QCD at low temperature. On the other hand the DQPM is based on a two-particle irreducible approach for complex “resummed” propagators and “resummed” couplings especially tuned to lattice QCD results from the Wuppertal-Budapest Collaboration for the entropy density $s(T)$ above temperatures of 140 MeV. In this respect the DQPM does not have a well defined effective lagrangian in the low temperature limit that might allow for an explicit calculation of cross sections, however, the interaction rates of the partons are included in the width of the spectral functions such that the various transport coefficients can be calculated in a straight forward manner. Unfortunately, the lattice QCD results from the two collaborations differ substantially due to the different implementations of the action and bare quark masses. Accordingly, the various comparisons have to be taken with care and not on an absolute scale.

We have seen that the NJL model does not reproduce the lattice QCD equations of state; first of all because the number of degrees of freedom is not sufficient in the vicinity of T_c but also because there is no explicit control on gluon degrees of freedom and their contribution to the thermodynamic potential. However, the results for the thermodynamic quantities $s(T)$, $P(T)$ etc. approximately decouple from the transport properties which appear reasonable in the vicinity of T_c up to about $1.5 T_c$ whereas the NJL fails to describe the transport coefficients in the high temperature phase for $T \geq 1.5 T_c$. Indeed, as confirmed by the relaxation time τ or by the shear viscosity to entropy density ratio η/s , the NJL model overestimates the interactions between the low mass constituent quarks in the medium at high temperature and lacks the gluon dynamics. The PNJL model performs better for the entropy and energy

density due the introduction of an explicit Polyakov loop potential that describes the pressure from the gluonic degrees of freedom as a function of temperature and leads to a narrower cross over region around T_c .

It is interesting to see that despite the small number of parameters of the NJL model, one can easily describe the thermodynamical properties as well as the transport coefficients within some deviation from LQCD results in equilibrium. Other models like the DQPM are designed to match LQCD results and are very useful to describe a realistic plasma with the right number of degrees of freedom, but this is not an effective lagrangian model where one can directly extract cross sections. We note in passing that this task can be solved to some extent within the PHSD transport approach which has been shown to match the DQPM results in thermodynamic equilibrium [53]. In any cases neither the (P)NJL model nor the DQPM can describe explicitly the dynamics of confinement.

The important message we want to point out here is that – although there is no perfect model to describe the physics of the QGP – there are effective approaches that reproduce thermodynamic as well as transport properties of QCD in equilibrium as shown by the explicit comparison to LQCD results. Furthermore, we have pointed out quantitatively the limitations of the models with respect to their applicability in energy density (or temperature) and provided ratios for transport coefficients that in principle can be well controlled by LQCD calculations. Further studies on the NJL model in a box, for equilibration times, strangeness dynamics and a mixed phase (in analogy to Ref. [26, 53]) are in progress.

XIII. ACKNOWLEDGMENT

We thank H. Hansen, D. Rischke, C. Sasaki, and N. N. Scoccola for illuminating discussions. We are also grateful to O. Linnyk and V. Ozvenchuk for providing various LQCD data points. We, furthermore, acknowledge support through the “HIC for FAIR” framework of the “LOEWE” program. The computational resources have been provided by the LOEWE-CSC.

-
- [1] P. Rehberg, S. Klevansky, and J. Hüfner, *Nucl.Phys.* **A608**, 356 (1996).
- [2] R. Marty and J. Aichelin, *Phys. Rev. C* **87**, 034912 (2013).
- [3] C. Ratti, S. Rößner, M. Thaler, and W. Weise, *Eur.Phys.J.* **C49**, 213 (2007).
- [4] A. Peshier, *Phys. Rev. D* **70**, 034016 (2004).
- [5] A. Peshier and W. Cassing, *Phys.Rev.Lett.* **94**, 172301 (2005).
- [6] W. Cassing, *The European Physical Journal Special Topics* **168**, 3 (2009).
- [7] W. Cassing and E. Bratkovskaya, *Phys.Rev.* **C78**, 034919 (2008).
- [8] E. Bratkovskaya, W. Cassing, V. Konchakovski, and O. Linnyk, *Nucl.Phys.* **A856**, 162 (2011).
- [9] W. Cassing and E. Bratkovskaya, *Nucl.Phys.* **A831**, 215 (2009).
- [10] Y. Nambu and G. Jona-Lasinio, *Phys. Rev.* **122**, 345 (1961).
- [11] S. Klevansky, *Rev.Mod.Phys.* **64**, 649 (1992).
- [12] P. Rehberg and S. Klevansky, *Annals of Physics* **252**, 422 (1996).
- [13] U. Vogl and W. Weise, *Progress in Particle and Nuclear Physics* **27**, 195 (1991).
- [14] R. Nebauer and J. Aichelin, *Phys.Rev.* **C65**, 045204 (2002).
- [15] M. Buballa, *Physics Reports* **407**, 205 (2005).
- [16] P. Costa, M. Ruivo, C. de Sousa, and Y. Kalinovsky, *Phys.Rev.* **D71**, 116002 (2005).
- [17] M. Thomere, Ph.D. thesis, Université de Nantes (2009).
- [18] K. Fukushima, *Phys.Lett.* **B591**, 277 (2004).
- [19] P. Costa, M. Ruivo, C. de Sousa, H. Hansen, and W. Alberico, *Phys.Rev.* **D79**, 116003 (2009).
- [20] P. Costa, M. Ruivo, C. de Sousa, and H. Hansen, *Symmetry* **2**, 1338 (2010).
- [21] H. Hansen, W. Alberico, A. Beraudo, A. Molinari, M. Nardi, *et al.*, *Phys.Rev.* **D75**, 065004 (2007).
- [22] A. Friesen, Y. Kalinovsky, and V. Toneev, *Int.J.Mod.Phys.* **A27**, 1250013 (2012).
- [23] O. Kaczmarek, F. Karsch, P. Petreczky, and F. Zantow, *Phys.Lett.* **B543**, 41 (2002).
- [24] S. Borsanyi, G. Endrodi, Z. Fodor, A. Jakovac, S. D. Katz, *et al.*, *JHEP* **1011**, 077 (2010).
- [25] L. P. Kadanoff and G. Baym, *Quantum Statistical Mechanics* (Benjamin, New York, 1962).
- [26] V. Ozvenchuk, O. Linnyk, M. Gorenstein, E. Bratkovskaya, and W. Cassing, (2012), [arXiv:1212.5393 \[hep-ph\]](https://arxiv.org/abs/1212.5393).
- [27] M. Bluhm, B. Kämpfer, and K. Redlich, *J.Phys.Conf.Ser.* **270**, 012062 (2011).
- [28] M. Cheng, S. Ejiri, P. Hegde, F. Karsch, O. Kaczmarek, *et al.*, *Phys. Rev. D* **81**, 054504 (2010).
- [29] Y. Aoki, Z. Fodor, S. Katz, and K. Szabo, *Phys.Lett.* **B643**, 46 (2006).
- [30] A. Bhattacharyya, P. Deb, S. K. Ghosh, R. Ray, and S. Sur, *Phys. Rev. D* **87**, 054009 (2013).
- [31] C. Sasaki and K. Redlich, *Nucl.Phys.* **A832**, 62 (2010).
- [32] C. Sasaki and K. Redlich, *Phys.Rev.* **C79**, 055207 (2009).
- [33] P. Zhuang, J. Hüfner, S. Klevansky, and L. Neise, *Phys.Rev.* **D51**, 3728 (1995).
- [34] H. B. Meyer, *Phys.Rev.* **D76**, 101701 (2007).
- [35] A. Nakamura and S. Sakai, *Phys. Rev. Lett.* **94**, 072305 (2005).
- [36] S. Sakai and A. Nakamura, *PoS LAT2007*, 221 (2007).
- [37] H. B. Meyer, *Phys.Rev.Lett.* **100**, 162001 (2008).
- [38] H. B. Meyer, *Nucl.Phys.* **A830**, 641C (2009).
- [39] P. Chakraborty and J. Kapusta, *Phys.Rev.* **C83**, 014906 (2011).
- [40] S. Plumari, A. Puglisi, F. Scardina, and V. Greco, *Phys.Rev.* **C86**, 054902 (2012).
- [41] P. K. Kovtun, D. T. Son, and A. O. Starinets, *Phys. Rev. Lett.* **94**, 111601 (2005).
- [42] H.-T. Ding, A. Francis, O. Kaczmarek, F. Karsch, E. Laermann, *et al.*, (2013), [arXiv:1301.7436 \[hep-lat\]](https://arxiv.org/abs/1301.7436).
- [43] G. Aarts, C. Allton, J. Foley, S. Hands, and S. Kim, *Phys. Rev. Lett.* **99**, 022002 (2007).
- [44] S. Gupta, *Phys.Lett.* **B597**, 57 (2004).
- [45] B. B. Brandt, A. Francis, H. B. Meyer, and H. Wittig, (2013), [arXiv:1302.0675 \[hep-lat\]](https://arxiv.org/abs/1302.0675).
- [46] F. Reif, *Fundamentals of Statistical and Thermal Physics* (McGraw-Hill, 1965).
- [47] W. Cassing, O. Linnyk, T. Steinert, and V. Ozvenchuk, *Phys. Rev. Lett.* **110**, 182301 (2013).
- [48] W. Israel and J. Stewart, *Annals of Physics* **118**, 341 (1979).
- [49] S. de Groot, W. van Leeuwen, and C. van Weert, *Relativistic Kinetic Theory: Principles and Applications* (North-Holland; Elsevier, Amsterdam; New York, 1980).
- [50] G. S. Denicol, H. Niemi, E. Molnár, and D. H. Rischke, *Phys. Rev. D* **85**, 114047 (2012).
- [51] M. Greif, F. Reining, I. Bouras, G. S. Denicol, Z. Xu, and C. Greiner, *Phys. Rev. E* **87**, 033019 (2013).
- [52] H. Heiselberg and C. Pethick, *Phys.Rev.* **D48**, 2916 (1993).
- [53] V. Ozvenchuk, O. Linnyk, M. Gorenstein, E. Bratkovskaya, and W. Cassing, *Phys.Rev.* **C87**, 024901 (2013).